Ferromagnetic Quantum Critical Point in the Heavy-Fermion Metal YbNi$_4$(P$_{1−x}$As$_x$)$_2$

Alexander Steppke,[1]* Robert Küchler,[1] Stefan Lausberg,[1] Edit Lengyel,[1] Lucia Steinke,[1] Robert Borth,[1] Thomas Lühmann,[1] Cornelius Krellner,[1,2] Michael Nicklas,[1] Christoph Geibel,[1] Frank Steglich,[1] Manuel Brando[1]*

Unconventional superconductivity and other previously unknown phases of matter exist in the vicinity of a quantum critical point (QCP): a continuous phase change of matter at absolute zero. Intensive theoretical and experimental investigations on itinerant systems have shown that metallic ferromagnets tend to develop via either a first-order phase transition or through the formation of intermediate superconducting or inhomogeneous magnetic phases. Here, through precision low-temperature measurements, we show that the Grüneisen ratio of the heavy fermion metallic ferromagnet YbNi$_4$(P$_{0.92}$As$_{0.08}$)$_2$ diverges upon cooling to $T = 0$, indicating a ferromagnetic QCP. Our observation that this kind of instability, which is forbidden in d-electron metals, occurs in a heavy fermion system will have a large impact on the studies of quantum critical materials.

Fluctuations of quantum fields persist to absolute zero. In matter, when such quantum fluctuations are tuned by a nonthermal control parameter such as pressure, they may become sufficiently large to cause a quantum phase transition into a new ground state. If the transition is continuous, it gives rise to a quantum critical point (QCP) (1–3). QCPs have been observed in a number of antiferromagnetic (AFM) d- and f-electron metallic systems (4, 5) but are thought not to exist in ferromagnetic (FM) metals for several reasons.

Theoretical considerations for itinerant (such as d-electron) systems exclude a FM QCP at field $H = 0$ in clean materials and rather point to a FM quantum phase transition of first order (6–9). Experiments indicate that FM QCPs are preempted by the development of superconducting (10, 11), modulated (12) or spin-glass–like (13) phases, or a first-order FM quantum phase transition (14). In f-electron systems, Kondo screening competes with magnetism and permits QCPs, at which the Kondo effect may even be destroyed, as shown in the AFM heavy-fermion metal YbRh$_2$Si$_2$ (15–17). For a FM f-derived Kondo-lattice system, it has been shown theoretically that the Kondo screening may completely disappear deep inside the ferromagnetically ordered phase (18). It remains to be shown, however, whether the FM QCP concurs also with a Kondo-destroying one.

An ideal method to probe the existence of a heavy fermion QCP (which is generically sensitive to pressure) is to perform combined measurements of the volume thermal expansion, $\beta(T)$, and specific heat, $C(T)$. Both $\beta(T)/T$ and $C(T)/T$

diverge upon approaching the QCP, but the divergence of $\beta(T)/T$ is stronger, leading to a divergence of the Grüneisen ratio $\Gamma(T) = \beta(T)/C(T)$. If the divergence of the Grüneisen ratio follows a power law, $\Gamma(T) \propto T^{-\lambda}$, the critical exponent yields insight into the nature of the QCP (19). For instance, in CeNi$_2$Ge$_2$ $\lambda = 1$ is observed, indicating a three-dimensional (3D) spin-density-wave QCP (20). For the unconventional quantum critical material YbRh$_2$Si$_2$, a fractional exponent, $\lambda \approx 0.7$, was found (20).

In this report, we show that in single crystals of the weak $4f$-derived metallic ferromagnet YbNi$_4$P$_2$, a FM QCP can be induced by applying negative chemical pressure—substituting 10% As

for P. At this QCP, $\beta(T)/T$, $C(T)/T$, and $\Gamma(T)$ diverge with unusual power-law exponents.

Stoichiometric FM metals with a Curie temperature T_C below 1 K are very rare. The Kondo-lattice system YbNi$_4$P$_2$ is one, with a remarkably low $T_C = 0.17$ K (21). This is mainly a result of substantial Kondo screening (with a Kondo temperature $T_K \approx 8$ K) of the magnetic Yb^{3+} ions [Ni is not magnetic (22)], leaving a FM ground state with a small ordered moment of ~0.05 Bohr magneton (μ_B) (23) and strongly enhanced electron-electron correlations (21). It is, therefore, a particularly suitable system to search for and explore FM quantum criticality.

A preliminary study on YbNi$_4$P$_2$ polycrystals, in which the low-temperature transition at T_C was discovered (21), indicated peculiar non-Fermi liquid (NFL) properties in transport and thermodynamic quantities above T_C: in particular, a stronger-than-logarithmically diverging Sommerfeld coefficient $C(T)/T$ and a linear T-dependence of the electrical resistivity $\rho(T)$. These results suggest the proximity of a FM QCP; T_C could be tuned smoothly to zero through the isoelectronic substitution of larger As for P, expanding the crystal lattice and causing, in Yb systems, an increase of T_K and a reduction of T_C (24). We report thermodynamic and transport measurements on single crystals of stoichiometric YbNi$_4$P$_2$ (23) as well as YbNi$_4$(P$_{1−x}$As$_x$)$_2$, with x between 0.04 and 0.13. YbNi$_4$P$_2$ has a crystalline structure of the tetragonal ZrFe$_4$Si$_2$ structure type ($P4_2/mnm$), with the Yb^{3+} ions located between chains of edge-connected Ni tetrahedra. The Yb ions form chains along the crystallographic c direction, with the lattice parameter $a = 7.0565$ Å being almost twice as large as $c = 3.5877$ Å (Fig. 1A, inset) (22). Band-structure calculations show that three sheets of the Fermi surface have
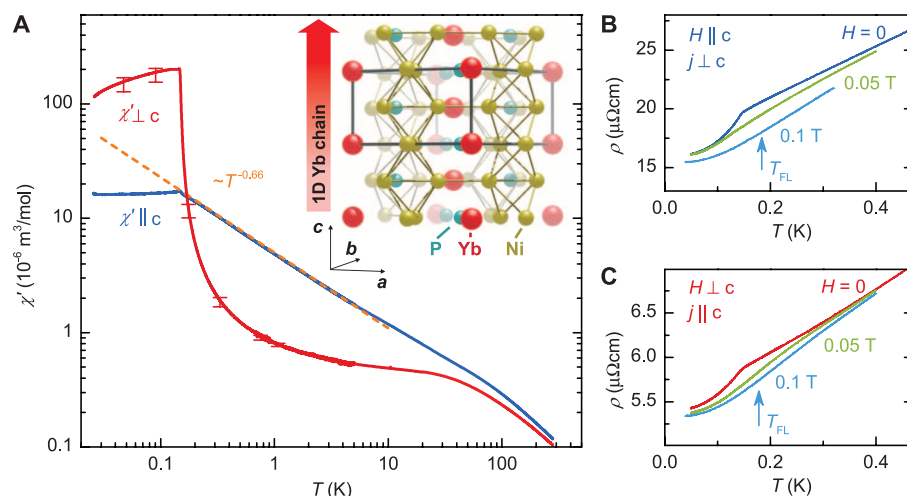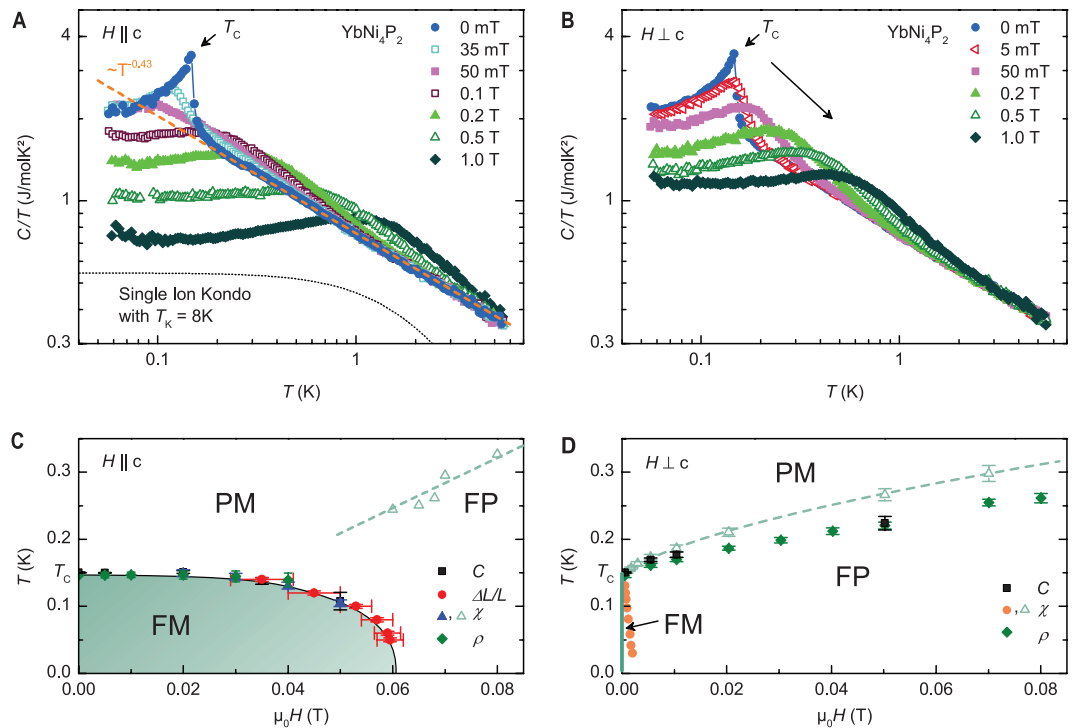

Fig. 1. Temperature dependence of the magnetic and electrical properties of YbNi$_4$P$_2$. (**A**) Real part of the magnetic susceptibility χ' plotted as a function of temperature, measured perpendicular ($\chi'_\perp$) and parallel ($\chi'_\parallel$) to the c axis. The orange dashed line emphasizes the $T^{-0.66}$ behavior of $\chi'_\parallel$ versus T below 10 K. (Inset) Unit cell of YbNi$_4$P$_2$. (**B** and **C**) Electrical resistivity ρ plotted as a function of temperature and measured with current j (B) perpendicular and (C) parallel to the crystallographic c axis. The kinks at T_C disappear at fields $\mu_0 H \geq 0.05$ T in both field directions. At a field of 0.1 T, both resistivities follow a temperature dependence close to T^2 below T_{FL} (arrows).

[1]Max Planck Institute for Chemical Physics of Solids, Nöthnitzer Strasse 40, 01187 Dresden, Germany. [2]Institute of Physics, Goethe University Frankfurt, Max-von-Laue-Strasse 1, 60438 Frankfurt am Main, Germany.

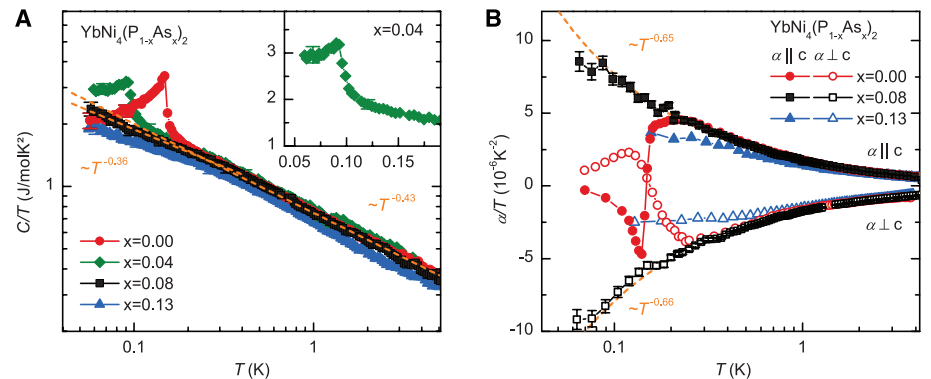*To whom correspondence should be addressed. E-mail: steppke@cpfs.mpg.de (A.S.); brando@cpfs.mpg.de (M.B.)

Fig. 2. Magnetic phase diagrams of $YbNi_4P_2$. (**A**) C/T versus T of $YbNi_4P_2$ measured at magnetic fields $H \parallel c$. The dashed orange line emphasizes the $T^{-0.43}$ power-law behavior observed above 0.2 K up to about 6 K. The dotted black line is the specific-heat contribution calculated within the single-ion $S = 1/2$ Kondo model of (25), with $T_K = 8$ K and C/T scaled by a factor of 0.5 for better visibility. (**B**) C/T versus T of $YbNi_4P_2$ measured at magnetic fields $H \perp c$. In (A) and (B), the nuclear Schottky contribution has been subtracted from the raw specific-heat data (32). (**C**) Magnetic phase diagram for $H \parallel c$, derived from equal-entropy construction for the phase-transition anomaly in the specific-heat coefficient [$C(T)/T$], kink in the linear magnetostriction $\Delta L(T)/L$ (fig. S10), inflection point of the ac-susceptibility, and first derivative of the resistivity [$\rho(T)$]. The paramagnetic (PM) region is separated from the ferromagnetic (FM) region, where the moments are aligned within the (a,b) plane, by a phase transition of the second order (solid black line). The dashed lines in (C) and (D) indicate the crossover between the PM and the ferromagnetically polarized (FP) regions, determined by the maxima in the ac-susceptibility (fig. S8). (**D**) Magnetic phase diagram for $H \perp c$ derived from $C(T)$, $\rho(T)$, and $\chi'(T)$. The vertical green line at $H = 0$ indicates that the FM order exists at $H = 0$ only. The orange circles mark the increase of $\chi'(T)$ below the crossover temperature (fig. S8).

a pronounced 1D character (21), which may be relevant to the understanding of the unusual NFL behavior of $YbNi_4P_2$. Because adjacent Yb chains are shifted by $c/2$, Yb^{3+} ions experience a crystalline electrical field (CEF) that is rotated by 90° from chain to chain, although the symmetry on each Yb site is the same. This causes frustration between neighboring chains, which together with strong electron-electron correlations may enhance the strength of quantum fluctuations.

We first focus on stoichiometric $YbNi_4P_2$. The strongest evidence of the FM order is provided by the real-part of the ac-susceptibility, $\chi'(T)$, measured both with field $H \parallel c$ ($\chi'_\parallel$) and $H \perp c$ ($\chi'_\perp$) (Fig. 1A). Although the CEF anisotropy results in a much larger ground-state moment along the c direction than in the (a,b) plane, the FM ordering is perpendicular to c. As T is lowered toward $T_C = (0.150 \pm 0.005)$ K, $\chi'_\perp$ increases sharply up to a value of $\sim 200 \times 10^{-6}$ m³/mol (≈ 4 in SI units). Below T_C, a pronounced increase of the imaginary part $\chi''_\perp$ of $\chi_{ac}(T)$ ($H \perp c$) is observed, representative of energy dissipation (fig. S7). In the same T region, $\chi'_\perp$ is only weakly T-dependent, possibly because the coercive field of the magnetic hysteresis is very small (21). $\chi'_\parallel$ increases with decreasing T, following a $T^{-0.66}$ power law below 10 K down to T_C, where it saturates at a value of $\sim 17 \times 10^{-6}$ m³/mol. This anisotropy of the susceptibility suggests that the spins align perpendicularly to the c direction, and $\chi'_\parallel$ measures the transversal fluctuations. Clear kinks are

seen at T_C in the resistivity curves $\rho_\perp(T)$ and $\rho_\parallel(T)$, with current j perpendicular (Fig. 1B) or parallel (Fig. 1C) to the c axis. Below T_C, the resistivity follows a T^n power law, with $n_\perp = 2.9$ and $n_\parallel = 2.5$, very likely because of charge-carrier scattering from FM magnons. As in the polycrystals, the resistivity is quasi-T-linear just above T_C. Such a NFL property, when observed over a

sufficiently extended temperature range, is commonly considered a hallmark of quantum criticality (1, 2, 15, 16). Because of the relatively low Kondo temperature, $T_K \approx 8$ K, a proper $\rho \sim T^n$ behavior is observed only within the rather narrow temperature window 0.15 K $\leq T \leq 1$ K. In this range, $\rho = \rho_0 + AT^n$, with $n_\perp = 1$ and $n_\parallel = 1.2$, and the coefficient $A_\perp = 21.6$ microhm·cm/K is

Fig. 3. Tuning T_C to zero by As substitution. (**A**) Specific heat $C(T)$ divided by T of $YbNi_4(P_{1-x}As_x)_2$ for indicated values of x at $H = 0$. With increasing x, the FM transition temperature is tuned to zero. For $x = 0.08$, C/T follows a $T^{-0.43}$ power law with a deviation below 0.25 K to $T^{-0.36}$ (orange dashed lines). (**B**) Linear thermal-expansion coefficient $\alpha(T)$ divided by T of $YbNi_4(P_{1-x}As_x)_2$ with $x = 0$, 0.08, and 0.13 measured in zero field along ($\alpha \parallel c$) and perpendicular ($\alpha \perp c$) to the c axis. Here, the orange dashed lines emphasize the $T^{-0.65}$ and $-T^{-0.66}$ power-law behavior of α/T versus T along the crystallographic c and a directions, respectively. For $YbNi_4(P_{0.87}As_{0.13})_2$, the coefficient $\alpha(T)/T$ tends to saturate below 1 K, indicating noncritical behavior.

Fig. 4. Quantum critical behavior in YbNi$_4$(P$_{1-x}$As$_x$)$_2$. (**A**) Low-temperature ac-susceptibility for $x = 0.08$, measured at $H = 0$, where a rounded maximum is visible at $T_C = 0.028$ K in $\chi'_\perp(T)$. (**B**) $T - x$ phase diagram: The FM QCP is located at $x_c \approx 0.1$. (**C**) Temperature dependence of C/T and β/T for the YbNi$_4$(P$_{0.92}$As$_{0.08}$)$_2$ sample, which is the sample closest to the FM QCP. Both quantities diverge with decreasing T as $C(T)/T \propto T^{-0.43}$ ($\propto T^{-0.36}$ below 0.25 K) and $\beta(T)/T \propto T^{-0.64}$. (Inset) Temperature dependence of the absolute value of the dimensionless Grüneisen ratio $\Gamma = V_{mol}/\kappa_T \cdot \beta/C$ for $x = 0.08$ [using the isothermal compressibility $\kappa_T = 5.3 \times 10^{-12}$ Pa^{-1} of YbRh$_2$Si$_2$ (33)] which reveals the presence of quantum critical fluctuations at the FM QCP. The dashed red line emphasizes the $T^{-0.22}$ divergence of $\Gamma(T)$ in zero field.
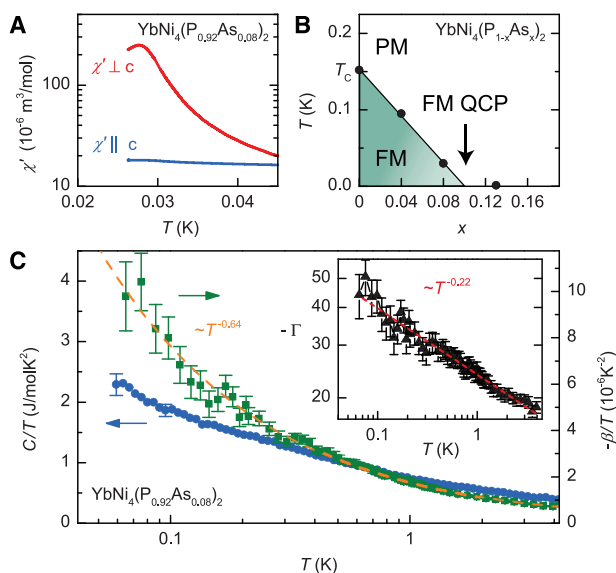
much larger than $A_\parallel = 3.8$ microhm·cm/K$^{1.2}$. This indicates a Fermi velocity that is much higher along the Yb chains than within the (a,b) plane, which is in accordance with the anisotropic Fermi surface (21).

Additional thermodynamic evidence of the phase transition at T_C and of the in-plane FM order is presented in Fig. 2, A and B, in which the T and H dependences of the specific heat are shown together with the result of the single-ion Kondo model (25). At $H = 0$, a sharp λ-type phase transition in C/T versus T is observed, associated with a small change of the molar 4f-derived entropy (1% of $R\ln2$, with $R = 8.31$ J/molK). A magnetic field applied parallel to the c axis shifts the transition temperature to lower T (Fig. 2A), whereas for $H \perp c$, the crossover to the polarized state is shifted to higher temperatures (Fig. 2B). This is corroborated by the H dependence of $\chi'(T)$ (fig. S8, A and B): For $H \perp c$, a sharp peak appears already at very low fields, where the system directly enters the polarized state, and then broadens at higher fields. The resulting magnetic phase diagrams are displayed in Fig. 2, C and D. These observations point to in-plane FM order in YbNi$_4$P$_2$, although neutron-diffraction experiments are required to determine the exact magnetic structure, which very likely is not collinear.

At $H = 0$, $C(T)/T$ increases below 6 K, following a $T^{-0.43\pm0.02}$ power law over a notably wide range down to 0.2 K, where classical thermal fluctuations associated with the phase transition set in. A similar power law [$C(T)/T \propto T^{-0.4}$] has been observed at the field-induced QCP of YbRh$_2$Si$_2$, an AFM system with strong FM fluctuations (15). For YbNi$_4$P$_2$, a pronounced λ-peak at T_C indicates a second-order phase transition. This, and the distinct NFL properties above T_C, suggest that this compound is located in the close vicinity of a QCP, where $T_C \rightarrow 0$ smoothly.

To approach the QCP, we used arsenic substitutions of $x = 0.04$, 0.08, and 0.13 in YbNi$_4$(P$_{1-x}$As$_x$)$_2$. The QCP is achieved at $x_c \approx 0.1$, as demonstrated by calorimetric and dilatometric results in Fig. 3, A and B, and in the phase diagram of Fig. 4B. For $x = 0.04$, the phase transition remains FM and second order (Fig. 3A, green diamonds); in fact, $C(T)/T$ of YbNi$_4$(P$_{0.96}$As$_{0.04}$)$_2$ has been measured at $H \perp c$, and the transition was found to be shifted to higher T with increasing H (fig. S6). For $x = 0.08$, $C(T)/T$ increases continuously down to 0.06 K, and no phase transition is detected. $C(T)/T$ can be described by the same T-dependence as for YbNi$_4$P$_2$ down to 0.25 K, where a slight deviation from this power law (to $T^{-0.36}$) is visible (Fig. 3A, orange dashed lines). Pronounced changes of the T-dependence of $C(T)/T$ and of the Grüneisen ratio $\Gamma(T)$ were observed in YbRh$_2$Si$_2$ below 0.3 K (5, 15, 20); in our case, this deviation results in only a minor change of $\Gamma(T)$ (figs. S12 and S13). Measurements of $\chi'(T)$ down to 0.02 K picked up a transition at 0.028 K, which is similar to the behavior observed in YbNi$_4$P$_2$ (Fig. 4A and fig. S9). This implies that, also for $x = 0.08$, the transition is FM and second order. For $x = 0.13$, no phase transition is observed, and $C(T)/T$ versus T seems to follow the same T dependence down to 0.1 K, but with smaller absolute values. This indicates that the same power-law divergence observed in $C(T)/T$ for the pure system is retained across x_c.

The observed NFL features suggest the presence of strong quantum fluctuations (12, 13, 26–29) but do not directly imply the existence of a FM QCP, that these fluctuations become critical at $x_c \approx 0.1$ (13, 29). One key experiment to provide direct evidence of quantum critical fluctuations is the combined measurement of the volume-thermal-expansion coefficient $\beta = \alpha_\parallel + 2\alpha_\perp$ (with

$\alpha_\parallel$ and $\alpha_\perp$ being the linear expansion coefficients along c and a, respectively) and the specific heat of the same crystal, with x as close as possible to x_c (19, 20). The Grüneisen ratio $\Gamma(T)$ at x_c should diverge as $T^{-1/\nu z}$ with parameters ν, the spatial correlation-length exponent, and z, the dynamical exponent (19).

Whereas for YbNi$_4$P$_2$, a change of sign in $\alpha(T)/T$ is clearly visible at T_C (Fig. 3B), as expected at a second-order phase transition (30), for YbNi$_4$(P$_{0.92}$As$_{0.08}$)$_2$, no sign change can be seen down to 0.06 K, in accordance with $T_C = 0.028$ K. Upon cooling, the ratios $\alpha_\parallel/T$ and $\alpha_\perp/T$ diverge with similar exponents, yielding $\beta(T)/T \propto T^{-0.64\pm0.02}$. Although this is consistent with 3D FM spin fluctuations (19), the power-law divergence of the Sommerfeld coefficient $C(T)/T$ is at odds with the expected logarithmic behavior, $C(T)/T \propto \log(1/T)$, for an itinerant 3D FM QCP (19). For $x = 0.13$, $\alpha(T)/T$ saturates below 1 K, indicating the crossover to a heavy Fermi liquid phase (31).

The key evidence for the FM QCP in YbNi$_4$(P$_{1-x}$As$_x$)$_2$ is summarized in Fig. 4C. At $x = 0.08$—very close to x_c—not only do both $C(T)/T$ and $\beta(T)/T$ diverge with power-law exponents $T^{-0.43}$ ($T^{-0.36}$ below 0.25 K) and $T^{-0.64}$, respectively, but the dimensionless Grüneisen ratio diverges as $\Gamma(T) \propto T^{-0.22\pm0.04}$ (Fig. 4C, inset). This strongly indicates the existence of a QCP at $x_c \approx 0.1$. The critical exponent $\lambda = -0.22$ rules out an itinerant QCP scenario because it leads to $\nu z \approx 5$, which is much larger than for itinerant FM systems ($\nu = 1/2$, $z = 3$).

The unexpected power-law exponents in all thermodynamic quantities, indicating the presence of strong FM quantum critical fluctuations, require new theoretical concepts beyond the itinerant spin-fluctuation theory (2). These concepts must take into account the localized nature of the Yb-4f states in the presence of very strong spin-orbit coupling when compared with the CEF. Further, the Kondo coupling of the 4f states to the conduction electrons must be considered. Isothermal measurements of the Hall coefficient on YbNi$_4$(P$_{1-x}$As$_x$)$_2$ with $x > \sim0.1$ under hydrostatic pressure would greatly help to investigate the exciting possibility that the FM QCP concurs with a localization-delocalization transition of the Yb-4f states, similar to what was reported for YbRh$_2$Si$_2$ at its AFM QCP (5, 16, 17). The extent to which the FM instability in As-doped YbNi$_4$P$_2$ is affected by the 1D character of the electronic structure must also be clarified.

References and Notes
1. P. Coleman, A. J. Schofield, *Nature* **433**, 226 (2005).
2. H. Löhneysen, A. Rosch, M. Vojta, P. Wölfle, *Rev. Mod. Phys.* **79**, 1015 (2007).
3. G. R. Stewart, *Rev. Mod. Phys.* **73**, 797 (2001).
4. A. Yeh *et al.*, *Nature* **419**, 459 (2002).
5. J. Custers *et al.*, *Nature* **424**, 524 (2003).
6. D. Belitz, T. R. Kirkpatrick, T. Vojta, *Phys. Rev. Lett.* **82**, 4707 (1999).
7. A. V. Chubukov, C. Pépin, J. Rech, *Phys. Rev. Lett.* **92**, 147003 (2004).
8. G. J. Conduit, A. G. Green, B. D. Simons, *Phys. Rev. Lett.* **103**, 207201 (2009).

9. D. Belitz, T. Kirkpatrick, T. Vojta, *Rev. Mod. Phys.* **77**, 579 (2005).
10. E. Hassinger, D. Aoki, G. Knebel, J. Flouquet, *J. Phys. Soc. Jpn.* **77**, 073703 (2008).
11. S. S. Saxena *et al.*, *Nature* **406**, 587 (2000).
12. M. Brando *et al.*, *Phys. Rev. Lett.* **101**, 026401 (2008).
13. T. Westerkamp *et al.*, *Phys. Rev. Lett.* **102**, 206404 (2009).
14. D. Belitz, T. R. Kirkpatrick, http://arxiv.org/abs/1204.0873.
15. P. Gegenwart, Q. Si, F. Steglich, *Nat. Phys.* **4**, 186 (2008).
16. Q. Si, F. Steglich, *Science* **329**, 1161 (2010).
17. H. Pfau *et al.*, *Nature* **484**, 493 (2012).
18. S. J. Yamamoto, Q. Si, *Proc. Natl. Acad. Sci. U.S.A.* **107**, 15704 (2010).
19. L. Zhu, M. Garst, A. Rosch, Q. Si, *Phys. Rev. Lett.* **91**, 066404 (2003).
20. R. Küchler *et al.*, *Phys. Rev. Lett.* **91**, 066405 (2003).
21. C. Krellner *et al.*, *New J. Phys.* **13**, 103014 (2011).
22. C. Krellner, C. Geibel, *J. Phys. Conf. Ser.* **391**, 012032 (2012).
23. J. Spehling *et al.*, *Phys. Rev. B* **85**, 140406 (2012).
24. A. L. Cornelius, J. S. Schilling, D. Mandrus, J. D. Thompson, *Phys. Rev. B* **52**, R15699 (1995).
25. K. D. Schotte, U. Schotte, *Phys. Lett. A* **55**, 38 (1975).
26. N. T. Huy *et al.*, *Phys. Rev. B* **75**, 212405 (2007).
27. R. P. Smith *et al.*, *Nature* **455**, 1220 (2008).
28. S. Jia *et al.*, *Nat. Phys.* **7**, 207 (2011).
29. C. Pfleiderer, P. Böni, T. Keller, U. K. Rössler, A. Rosch, *Science* **316**, 1871 (2007).
30. M. Garst, A. Rosch, *Phys. Rev. B* **72**, 205129 (2005).
31. P. Thalmeier, B. Lüthi, in *Handbook on the Physics and Chemistry of Rare Earths*, K. A. Gschneidner Jr., L. Eyring, Eds. (North-Holland, New York, 1991), vol. 14, chap. 96, pp. 225–341.
32. Materials and methods are available as supplementary materials on *Science* Online.
33. J. Plessel *et al.*, *Phys. Rev. B* **67**, 180403 (2003).

Living Crystals of Light-Activated Colloidal Surfers

Jeremie Palacci,[1]* Stefano Sacanna,[1] Asher Preska Steinberg,[2] David J. Pine,[1] Paul M. Chaikin[1]

Spontaneous formation of colonies of bacteria or flocks of birds are examples of self-organization in active living matter. Here, we demonstrate a form of self-organization from nonequilibrium driving forces in a suspension of synthetic photoactivated colloidal particles. They lead to two-dimensional "living crystals," which form, break, explode, and re-form elsewhere. The dynamic assembly results from a competition between self-propulsion of particles and an attractive interaction induced respectively by osmotic and phoretic effects and activated by light. We measured a transition from normal to giant-number fluctuations. Our experiments are quantitatively described by simple numerical simulations. We show that the existence of the living crystals is intrinsically related to the out-of-equilibrium collisions of the self-propelled particles.

Self-organization often develops in thermal equilibrium as a consequence of entropy and potential interactions. However, there are a growing number of phenomena where order arises in driven, dissipative systems, far from equilibrium. Examples include "random organization" of sheared colloidal suspensions (*1*) and rods (*2*), nematic order from giant-number fluc-tuations in vibrated rods (*3*), and phase separation from self-induced diffusion gradients (*4*). Biological (*5–7*) and artificial active particles (*8–11*) also exhibit swarm patterns that result from their interactions (*12–15*).

In order to study active, driven, collective phenomena, we created a system of self-propelled particles where the propulsion can be turned on and off with a blue light. This switch provides rapid control of particle propulsion and a convenient means to distinguish nonequilibrium activity from thermal Brownian motion. Further, the particles are slightly magnetic and can be stabilized and steered by application of a modest magnetic field. Our system consists of an

[1]Department of Physics, New York University, 4 Washington Place, New York, NY 10003, USA. [2]Department of Physics and Chemistry, Brandeis University, Waltham, MA 02453, USA.

*To whom correspondence should be addressed. E-mail: jp153@nyu.edu

Fig. 1. (**A**) Scanning electron microscopy (SEM) of the bimaterial colloid: a TPM polymer colloidal sphere with protruding hematite cube (dark). (**B**) Living crystals assembled from a homogeneous distribution (inset) under illumination by blue light. (**C**) Living crystals melt by thermal diffusion when light is extinguished: Image shows system 10 s after blue light is turned off (inset, after 100 s). (**D** to **G**) The false colors show the time evolution of particles belonging to different clusters. The clusters are not static but rearrange, exchange particles, merge (D→F), break apart (E→F), or become unstable and explode (blue cluster, F→G). For (B) to (G), the scale bars indicate 10 μm. The solid area fraction is $\Phi_s \approx 0.14$.